

GaAs photonic crystal slab nanocavities: Growth, fabrication, and quality factor

J. Sweet^{a,*}, B.C. Richards^a, J.D. Olitzky^a, J. Hendrickson^a, G. Khitrova^a,
H.M. Gibbs^a, D. Litvinov^b, D. Gerthsen^b, D.Z. Hu^c, D.M. Schaadt^c,
M. Wegener^c, U. Khankhoje^d, A. Scherer^d

^a College of Optical Sciences, The University of Arizona, 1630 E. University Blvd., Tucson, AZ 85721, United States

^b Laboratorium für Elektronenmikroskopie, Universität Karlsruhe (TH), Wolfgang-Gaede-Strasse 1, D-76131 Karlsruhe, Germany

^c Institut für Angewandte Physik and DFG-Center for Functional Nanostructures (CFN), Universität Karlsruhe (TH),
Wolfgang-Gaede-Strasse 1, D-76131 Karlsruhe, Germany

^d Department of Electrical Engineering, California Institute of Technology, 1200 E California Blvd.,
Pasadena, CA 91125, United States

Received 29 July 2009; received in revised form 1 October 2009; accepted 23 October 2009

Available online 3 November 2009

Abstract

In an effort to understand why short wavelength (~ 1000 nm) GaAs-based photonic crystal slab nanocavities have much lower quality factors (Q) than predicted (and observed in Si), many samples were grown, fabricated into nanocavities, and studied by atomic force, transmission electron, and scanning electron microscopy as well as optical spectroscopy. The top surface of the AlGaAs sacrificial layer can be rough even when the top of the slab is smooth; growth conditions are reported that reduce the AlGaAs roughness by an order of magnitude, but this had little effect on Q . The removal of the sacrificial layer by hydrogen fluoride can leave behind a residue; potassium hydroxide completely removes the residue, resulting in higher Q s.

© 2009 Elsevier B.V. All rights reserved.

PACS : 81.07.b; 42.70.Qs

Keywords: Nanostructure fabrication; Microcavities; Photonic crystals; Integrated optics devices; Photonic integrated circuits

The small volume of a photonic crystal slab nanocavity makes it attractive for low-threshold lasing [1] and, with high-quality-factor designs [2], for semiconductor quantum optics, especially strong coupling between a single quantum dot and a single cavity mode [3–9]. The quality factor Q (cavity frequency ν divided by FWHM cavity linewidth) in a few cases has exceeded 15,000 [3,8,10,11] for fabrica-

tions on samples intended for strong coupling. More typically it is less than 10,000, particularly for the wavelength λ in the range 900–1000 nm where Si detectors greatly improve measurements. Very high- Q values have been computed for various cavity designs, but fabricated Q s are always much higher in silicon than in the GaAs system. In fact, a Q of 45,000 was already reported [2] in silicon for the L3 design used in [3] and throughout this article; optimization of that design has yielded 150,000 computationally [12] and 110,000 experimentally in Si (1.5 μm) [13]. This paper reports that whereas reducing the roughness of the top of the AlGaAs sacrificial layer did not improve Q noticeably,

* Corresponding author. Tel.: +1 520 548 4107;
fax: +1 866 705 9514.

E-mail address: jsweet@optics.arizona.edu (J. Sweet).

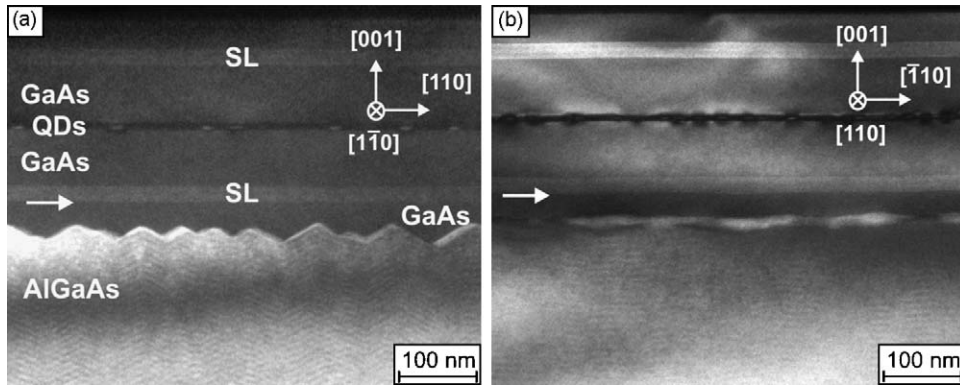


Fig. 1. (0 0 2) dark-field cross-section TEM images of PC sample showing that AlGaAs (light) roughness is greater along (a) [1 1 0] than (b) [-1 1 0]. The growth of GaAs (dark) almost flattens the surface by the time the first superlattice (SL) is grown (see arrows). The growth sequence of PC: GaAs buffer, ~700 nm $\text{Al}_{0.94}\text{Ga}_{0.06}\text{As}$ grown as a superlattice, 37.5 nm GaAs, 17.5 nm superlattice, 70 nm GaAs, 7.8 nm InGaAs quantum well with a layer of InAs quantum dots one-quarter in, 70 nm GaAs, 17.5 nm superlattice, and 37.5 nm GaAs.

using potassium hydroxide (KOH) to remove debris left behind in etching away the AlGaAs sacrificial layer did increase Q appreciably.

1. Reducing roughness at the top of the AlGaAs sacrificial layer

One of the diagnostics that can be used to evaluate a sample before fabrication is to scan the surface by atomic force microscopy (AFM). Scans ($40\ \mu\text{m} \times 40\ \mu\text{m}$) of our samples typically gave root mean square (r.m.s.) values around 1 nm, indicating smooth top surfaces consistent with scanning electron microscopy (SEM) images of the fabricated nanocavities. Cross-section transmission electron microscopy (TEM) images of the sample used for our initial observation of vacuum Rabi splitting [3] revealed that the AlGaAs/GaAs interface is rough; see Fig. 1. TEM images of three of our samples grown for fabrication in the 900–1000 nm wavelength range looked almost as rough. The smoothing accomplished by growth of the first few monolayers of GaAs helped to conceal this problem, as shown in Fig. 1 – which also shows that the roughness is much larger along [1 1 0] than along [1 -1 0].

What characteristics must the sacrificial layer have? The Al content x of the $\text{Al}_x\text{Ga}_{1-x}\text{As}$ needs to be in the range between 0.55 and 0.90 for etching with hydrofluoric (HF) acid. For $x > 0.90$ the etch rate is so fast that it is impractical to use an HF etch; steam oxidation of the AlGaAs in a furnace permits the use of a KOH wet etch, but it also introduces another step in fabrication which can be avoided by choosing a lower Al content. For $x < 0.55$ the etch rate is impractically slow. The AlGaAs needs to be thick enough to prevent light leakage to the substrate once the sacrificial layer

has been removed; a thickness of 800–1000 nm is often used for $900 < \lambda < 1200$ nm of interest here. The growth of smooth AlAs layers in Bragg mirror structures in vertical cavity surface emitting lasers (VCSELs) and planar microcavities is easier; the AlAs layer is typically only 70 nm thick and alternates with a similar thickness GaAs layer which smoothens any roughness at the top of the AlAs layer. The growth of smooth $\text{Al}_x\text{Ga}_{1-x}\text{As}$ in heterojunction lasers is also easier because x rarely exceeds 0.4.

Once the AlGaAs roughness was discovered, a quick and effective approach was taken to optimize the molecular beam epitaxy (MBE) growth: stop after growing $\text{Al}_x\text{Ga}_{1-x}\text{As}$, immediately remove the sample, and scan it by AFM. Growth parameters investigated included introducing a growth interruption to give time for smoothing under As, growing a thin layer of GaAs, and using a misoriented substrate. Most structures can be grown as well on a flat substrate as on one polished with the normal to the surface tilted a few degrees toward a particular crystal axis. However, it is known that the growth of AlGaAs is preferentially along step edges lying along [1-10]. If the surface is perfectly flat, then the surface diffusion may be inadequate to reach such an edge and island formation and 3D growth can result. This is consistent with Fig. 1 where it was found that the AlGaAs surface is rougher along [1 1 0] than along [1 -1 0]. Therefore, if one has not yet identified the ideal conditions for growth on a flat substrate, growth on a tilted substrate may be flatter. Consequently, growth on (0 0 1) GaAs substrates misoriented by 2° toward [1 1 0] was tried. As summarized in Table 1, several samples grown under approximately the same conditions showed that using a tilted substrate instead of a flat substrate and increasing the number of monolayers of GaAs always

Table 1
Summary of samples, growth parameters, and resulting surface.

| Sample | x | Periods | AlGaAs (nm) | GaAs (ML) | GI (s) | Cut ($^{\circ}$) | r.m.s. (nm) |
|--------|------|---------|-------------|-----------|--------|--------------------|-------------|
| QD24 | 0.7 | 1 | 1000 | 0 | 0 | 0 | 1.27* |
| QD29 | 0.7 | 12 | 100 | 7 | 120 | 0 | 0.83* |
| QD30 | 0.7 | 10 | 100 | 0.5 | 120 | 2 | 3.5 |
| QD31 | 0.7 | 1 | 1000 | 0 | 0 | 0 | 27 |
| QD33 | 0.5 | 1 | 10 | 0 | 0 | 0 | 0.69 |
| QD35 | 0.52 | 100 | 10 | 2 | 21 | 0 | 1.86 |
| QD37 | 0.51 | 100 | 10 | 2 | 21 | 2 | 1.14 |
| QD38 | 0.8 | 81 | 10 | 0.5 | 21 | 0 | 3.8 |
| QD39 | 0.75 | 80 | 10 | 0.7 | 21 | 2 | 2.0 |
| QD41 | 0.75 | 80 | 10 | 0.5 | 21 | 2 | 1.14* |
| A0947 | 0.55 | 80 | 10 | 0.85 | 21 | 0 | 1.3 |
| A0950 | 0.75 | 5 | 160 | 0 | 60 | 0 | 0.41 |
| A0961 | 0.75 | 2 | 400 | 0.5 | 120 | 0 | 0.4* |

Notation: “ x ” is Al concentration in AlGaAs; “Periods” is the number of times the sequence AlGaAs, GaAs, growth interruption was repeated; “AlGaAs” is the thickness of AlGaAs grown before the growth of GaAs of thickness “GaAs” (“ML” is monolayer = 0.283 nm) followed by a growth interruption of duration “GI”; “Cut” is the substrate misorientation angle; the root mean square AFM surface roughness is “r.m.s.”, and values marked with an asterisk (*) indicate the top of the GaAs slab, not grown on the other samples. QD31, grown like the AlGaAs in QD24, is representative of our AlGaAs before the present study.

decreased the r.m.s. value. However, the GaAs thickness needs to be less than one monolayer (ML) for good etching of the sacrificial layer. It was also found that decreasing the ratio of the As flux to the sum of the Al and Ga fluxes from 26 to 13 decreased the roughness. The results discussed so far were for samples grown in Tucson using a Riber 32 MBE machine. The substrate temperature was 570–580 $^{\circ}$ C. The Al concentration x was changed by varying the Ga flux, holding the Al flux constant; the AlGaAs growth rate was about 0.63 (0.86) ML/s for $x = 0.75$ (0.55). Even flatter AlGaAs was grown on a Riber Compact 21 MBE machine at the University of Karlsruhe (samples beginning with “A” in Table 1). There the growth rate was about 0.858 ML/s calibrated by reflection high energy electron diffraction (RHEED) oscillations, and the As_4 pressure was typically

8×10^{-4} Pa, roughly half that used in Tucson ($(1.5\text{--}2.1) \times 10^{-4}$ Pa). RHEED patterns were observed several times during each growth to monitor flatness and to keep the V/III flux ratio close to but above the transition to Ga-stabilized surface structure, leading to flatter growth.

2. Q values of nanocavities with smoother AlGaAs

Having determined growth conditions for AlGaAs flatter by an order of magnitude, we began growing complete structures, i.e., slabs on top of the $Al_xGa_{1-x}As$. For examples, see QD41 and A0961 in Table 1, where the r.m.s. values are now for the top of the GaAs slab. The TEM images in Fig. 2 verify that the AlGaAs is much flatter than in Fig. 1. The nanocavity Q

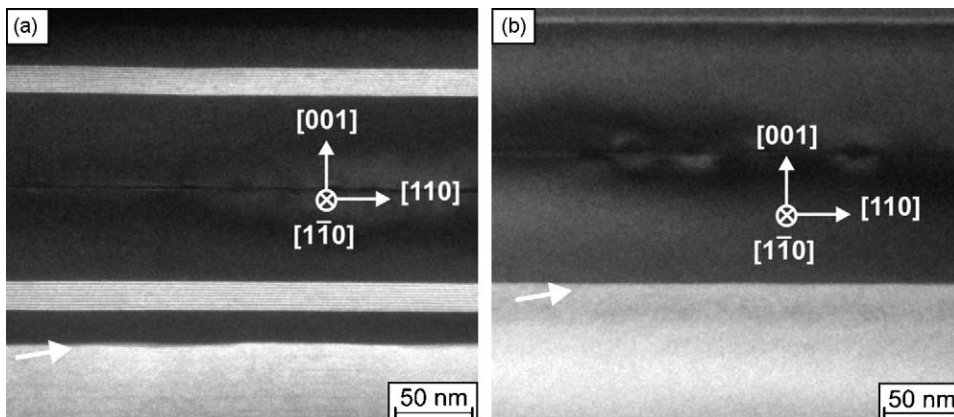


Fig. 2. (0 0 2) dark-field cross-section TEM images of (a) QD41 and (b) A0961 showing successful growth of flatter AlGaAs sacrificial layers (marked by arrows).

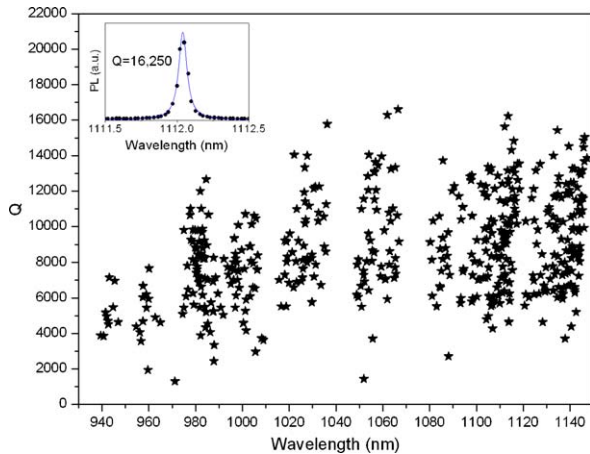


Fig. 3. Quality factors versus wavelength for A0961-3; cavities with $Q < 4000$ were not measured usually. The inset shows the photoluminescence spectrum for one of the highest Q s, and the blue curve is a Lorentzian fit to the data.

values of these samples were measured via their photoluminescence spectra with cw nonresonant excitation at 780 nm. The fabrication run A0961-3 yielded the Q values plotted in Fig. 3; a Q of 16,250, one of the highest Q s found, is shown in the inset. For comparison, the highest Q value obtained on rough-AlGaAs samples for $\lambda < 1000$ nm was 9000, whereas it reached 20,000 at $\lambda \cong 1200$ nm [10]. Therefore the data in Fig. 3 spanning 200 nm are consistent with the disjoint rough-AlGaAs data. This agreement means that taking the trouble to grow smoother AlGaAs did not improve the Q with our present fabrication quality. Fig. 3 shows little change in Q for wavelengths longer than 1020 nm, suggesting that Q may be limited by

non-vertical holes or fluctuations of hole shapes rather than Rayleigh scattering from imperfections which should increase as λ^4 . QD ensemble absorption and surface state absorption may cause the reduction in Q for short wavelengths.

3. KOH dip

The results just described for A0961-3 were obtained after the fabricated sample was dipped in a KOH solution (25 g/100 ml of deionized water) for 140 s just before it was placed in the cryostat and evacuated. This last step was added after an inspection of the SEM micrographs (Fig. 4a) revealed the presence of a semi-transparent object partially covering two holes in the upper left of the micrograph. AFM scans (Fig. 5) revealed the density and height variation of the debris and confirmed the hypothesis that this debris had floated and settled on the top of the slab after a successful dry etch. Speculating that this debris originated during the wet etch in the HF acid solution (1:10 = HF:H₂O by volume) and was probably a hydroxide of aluminum, we dipped the sample in a KOH solution. As is evident from the AFM scans, this process removed the debris completely. The effect of the KOH cleaning of surface debris on 10 different cavities was pronounced, showing an average improvement of 50%. One particular nanocavity from fabrication run A0961-3 showed a 73% improvement in Q from 4500 to 7800. Photoluminescence intensity also increased substantially, and the cavity modes shifted to higher energy on average 11 meV for all KOH treated cavities; see Fig. 4b for typical data.

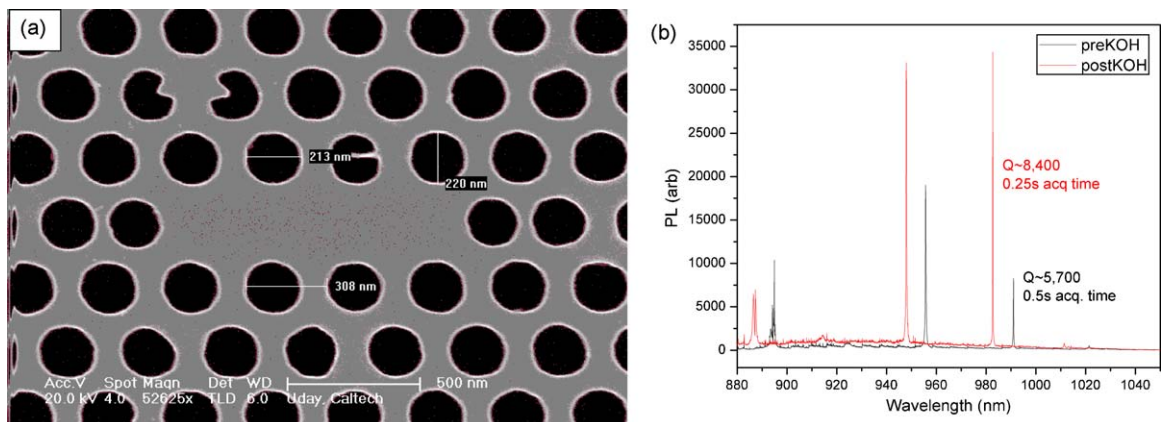


Fig. 4. (a) SEM image of part of one nanocavity in the fabrication run A0961-3 after O₂ plasma cleaning but before KOH cleaning. The lighter colored debris can be seen partially covering holes two and three in the second row and in several other locations. (b) Microphotoluminescence from a particular nanocavity of the fabrication run A0961-3 before and after KOH cleaning.

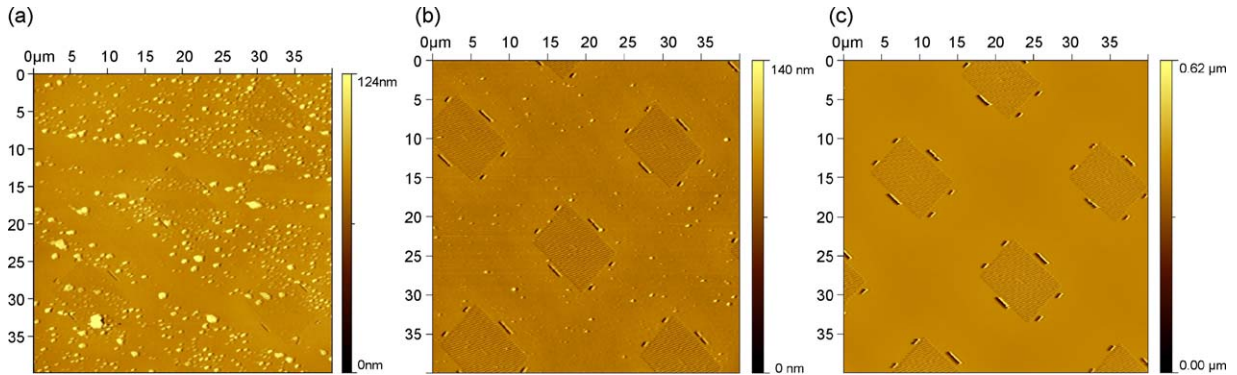


Fig. 5. AFM images of a few nanocavities of the fabrication run A0961-2 after O_2 plasma cleaning and (a) before swishing in a KOH solution (1.25 g KOH in 10 ml H_2O), (b) after 60 s, and (c) after 140 s. The bright yellow spots in (a) and (b) are debris that exceed 50 nm in height; the one in the bottom left corner of (a) exceeds 600 nm.

4. Summary

It was discovered by TEM that the top of the high-Al AlGaAs sacrificial layer in many of our MBE samples grown for fabrication of photonic crystal slab nanocavities is rough – even though the top surface of the sample (the top of the GaAs slab) is relatively flat, as had already been determined by AFM. MBE growth conditions were found that decrease the AlGaAs roughness by more than an order of magnitude. The improved smoothness will eventually be important for fabrication of high- Q nanocavities although its contribution at present is small. In addition, the efficacy of KOH in removing residue left behind in etching away the sacrificial layer is demonstrated.

Acknowledgements

HMG and GK would particularly like to thank Art Gossard and Mark Wistey for very helpful comments and suggestions on MBE growth of AlGaAs and L.C. Andreani for useful discussions on disorder. The USA authors would like to acknowledge support (EEC-0812072) from the National Science Foundation (NSF) through the Engineering Research Center for Integrated Access Networks (CIAN). The Tucson group also acknowledges support from NSF Atomic Molecular and Optical Physics (AMOP) and Electronics, Photonics and Device Technologies (EPDT), AFOSR, and Arizona Technology & Research Initiative Funding (TRIF). HMG thanks the Alexander von Humboldt Foundation for a Renewed Research Stay. The Caltech authors gratefully acknowledge critical support and infrastructure provided for this work by the Kavli

Nanoscience Institute at Caltech. The Karlsruhe researchers acknowledge financial support from the Deutsche Forschungsgemeinschaft (DFG) and the State of Baden-Württemberg through the DFG-Center for Functional Nanostructures (CFN) within subprojects A1.4 and A2.6.

References

- [1] O. Painter, R.K. Lee, A. Scherer, A. Yariv, J.D. O'Brien, P.D. Dapkus, I. Kim, Two-dimensional photonic band-gap defect mode laser, *Science* 284 (1999) 1819–1821.
- [2] Y. Akahane, T. Asano, B.S. Song, S. Noda, High- Q photonic nanocavity in a two-dimensional photonic crystal, *Nature* 425 (2003) 944–947.
- [3] T. Yoshie, A. Scherer, J. Hendrickson, G. Khitrova, H.M. Gibbs, G. Rupper, C. Ell, O.B. Shchekin, D.G. Deppe, Vacuum Rabi splitting with a single quantum dot in a photonic crystal nanocavity, *Nature* 432 (2004) 200–203.
- [4] J.P. Reithmaier, G. Sek, A. Löffler, C. Hofmann, S. Kuhn, S. Reitzenstein, L.V. Keldysh, V.D. Kulakovskii, T.L. Reinecke, A. Forchel, Strong coupling in a single quantum dot-semiconductor microcavity system, *Nature* 432 (2004) 197–200.
- [5] G. Khitrova, H.M. Gibbs, M. Kira, S.W. Koch, A. Scherer, Vacuum Rabi splitting in semiconductors, *Nat. Phys.* 2 (2006) 81–90.
- [6] K. Hennessy, A. Badolato, M. Winger, D. Gerace, M. Atature, S. Gulde, S. Falt, E.L. Hu, A. Imamoglu, Quantum nature of a strongly coupled single quantum dot-cavity system, *Nature* 445 (2007) 896–899.
- [7] D. Englund, A. Faraon, I. Fushman, N. Stoltz, P. Petroff, J. Vučković, Controlling cavity reflectivity with a single quantum dot, *Nature* 450 (2007) 857–861.
- [8] M. Winger, A. Badolato, K.J. Hennessy, E.L. Hu, A. Imamoglu, Quantum dot spectroscopy using cavity quantum electrodynamics, *Phys. Rev. Lett.* 101 (2008) 226808.
- [9] S.M. Thon, M.T. Rakher, H. Kim, J. Gudat, W.T.M. Irvine, P.M. Petroff, D. Bouwmeester, Strong coupling through optical positioning of a quantum dot in a photonic crystal cavity, *Appl. Phys. Lett.* 94 (2009) 111115.

- [10] J. Hendrickson, B.C. Richards, J. Sweet, S. Mosor, C. Christenson, D. Lam, G. Khitrova, H.M. Gibbs, T. Yoshie, A. Scherer, O.B. Shchekin, D.G. Deppe, Quantum dot photonic-crystal-slab nanocavities: quality factors and lasing, *Phys. Rev. B* 72 (2005) 193303.
- [11] I. Fushman, D. Englund, A. Faraon, J. Vučković, Probing the interaction between a single quantum dot and a photonic crystal cavity, *Phys. Status Solidi (c)* 5 (2008) 2808–2815.
- [12] L.C. Andreani, D. Gerace, A. Agio, Gap maps, diffraction losses, and exciton-polaritons in photonic crystal slabs, *Photon. Nanostruct.* 2 (2004) 103–110.
- [13] M. Galli, S.L. Portalupi, M. Belotti, L.C. Andreani, L. O’Faolain, T.F. Krauss, Light scattering and Fano resonances in high- Q photonic crystal nanocavities, *Appl. Phys. Lett.* 94 (2009) 071101.